Research Square

Preprints are preliminary reports that have not undergone peer review.
They should not be considered conclusive, used to inform clinical practice,
or referenced by the media as validated information.

Substrate compliance modulates sperm flagellar beating

Shobitha Unnikrishnan
North Carolina Agricultural and Technical State University
Izabele Heyward
North Carolina Agricultural and Technical State University
Robert Scott
North Carolina Agricultural and Technical State University
Macie Jones
North Carolina Agricultural and Technical State University
Sajal Chakraborty
North Carolina Agricultural and Technical State University
Khadim Mbacke
North Carolina Agricultural and Technical State University
Leah Worrill
North Carolina Agricultural and Technical State University
Mohammad Azad
North Carolina Agricultural and Technical State University
Salil Desai
North Carolina Agricultural and Technical State University
Chih Kuan Tung
ctung@ncat.edu

North Carolina Agricultural and Technical State University

Article

Keywords:

Posted Date: November 9th, 2026

DOI: https://doi.org/10.21203/rs.3.rs-11395343/v1

License: This work is licensed under a Creative Commons Attribution 4.0 International License.
Read Full License

Additional Declarations: No competing interests reported.

Substrate compliance modulates sperm flagellar beating

Shobitha Unnikrishnan[1], Izabele Heyward[2], Robert L Scott[1], Macie Jones[1], Sajal Chakraborty[3], Khadim Mbacke[1], Leah Worrill[4], Mohammad A Azad[5], Salil Desai[2], and Chih Kuan Tung[1*]

Abstract

Sperm motility is significantly influenced by the physical environment of the female reproductive tract, where sperm move in proximity to the epithelium (with an estimated modulus of ~1–10 kPa) and within a viscoelastic fluid, such as mucus. Conventional semen analyses are conducted on rigid glass surfaces that do not reflect the softness of the tissues that line the female reproductive tract. Here, we investigated how substrate compliance changes bovine sperm motility and flagellar dynamics using polyethylene glycol diacrylate (PEGDA)-based hydrogel substrates with physiological stiffness and compared sperm behavior on these compliant surfaces with that on glass and polydimethylsiloxane (PDMS), both in identical viscoelastic fluids. Using high-speed imaging and automated flagellar tracking to quantify trajectory dynamics and flagellar beating waveforms, we observed that compliant substrates altered flagellar beating, characterized by reduced beat frequency and increased waveform amplitude compared with rigid substrates. We also found that despite substantial differences in flagellar beating across substrates, wave-propagation speed remained similar. Together, these findings demonstrate that the mechanical compliance of the solid environment changes flagellar dynamics, highlighting the need to incorporate substrate mechanical properties into sperm motility research and clinical assessments.

[1] Department of Physics, North Carolina A&T State University, Greensboro, NC, USA.
[2] College of Engineering, North Carolina A&T State University, Greensboro, NC, USA.
[3] Applied Science & Technology, North Carolina A&T State University, Greensboro, NC, USA
[4] Department of Biology, North Carolina A&T State University, Greensboro, NC, USA.
[5] Department of Chemical, Biological & Bioengineering, North Carolina A&T State University, Greensboro, NC, USA.
*Correspondence to: ctung@ncat.edu.

Introduction

To fertilize the egg, mammalian sperm must migrate through the complex, confined environment of the female reproductive tract[1,2]. During this journey, sperm encounter complex biological fluids, including viscoelastic, mucin-rich mucus, and flow within narrow lumens bounded by soft biological tissues[1,3]. Fluid flow and surface topography guide sperm migration and alter motility in these environments[1,4,5]. Sperm movement in vivo is therefore not merely swimming through an unbounded fluid but rather involves locomotion within a dynamic physical environment shaped by fluid rheology, flow, confinement, and nearby interfaces. The inner surfaces of the bovine cervix and uterotubal junction are lined with longitudinally oriented microgrooves, within which sperm have been observed to migrate[4,6]. Within the uterus, the limited luminal space makes surface interactions crucial, and wall effects may promote sperm accumulation near the entrance of the uterotubal junction[7]. As sperm progress to the oviduct, they migrate along narrow, highly branched passages and remain closely associated with the epithelial surface[8]. Therefore, sperm migration occurs primarily near biological tissue boundaries within the reproductive tract.

Boundary interactions can strongly influence sperm behavior. Mammalian sperm have long been known to swim close to surfaces, and boundary proximity influences orientation, trajectories, swimming speed, and flagellar motion[5,9,10]. These behaviors are attributed to hydrodynamic interactions with the boundary, as well as boundary geometry and short-range forces with surfaces[5,11-15]. Experimental observations show that sperm swimming within approximately 1 μm of a surface can transition to a predominantly planar flagellar beat, and this near-surface behavior is further influenced by the viscosity of the surrounding fluid[16]. In these cases, a non-deforming solid surface serves as a boundary condition for both the surrounding fluid and the swimmer by modifying fluid-mediated interactions and also constraining the swimmer by exerting a normal force. Our recent work with polymeric solutions demonstrated strong interactions between the flagellum and a solid surface via flagellum surface friction, contributing to propulsion through a hybrid motility mechanism in which fluid-mediated propulsion is complemented by surface contact[17]. We also found that a distinct mechanical interaction can arise when a substrate deforms. Specifically, we observed that the terminal bend of the flagella remained stationary in the laboratory frame on a more deformable PDMS substrate but not on glass, a difference that may arise from local flagellum-induced substrate indentation and the associated normal force[18]. Together, these findings indicate that boundaries can influence sperm propulsion beyond their role as mere geometric constraints and fluid boundary conditions. However, established surface interactions have been studied primarily on rigid substrates, which differ in mechanical properties from the soft tissue surfaces sperm encounter in the female reproductive tract; therefore, the consequences of substrate mechanical compliance for sperm motility remain largely unexplored.

If the mechanical properties of a substrate influence sperm motion, the flagellar waveform provides a direct route for such an effect to emerge. The flagellar beat is generated by the action of dynein motors organized along the axoneme, which drive relative sliding between adjacent microtubule doublets. Structural constraints within the axoneme convert this sliding into bending, resulting in a propagating mechanical wave along the flagellum.[19,20]. The resulting waveform arises from the combined action of active axonemal forces, passive flagellar elasticity, and mechanical resistance imposed by the

surrounding environment[21]. Beyond generating force, dynein motors are also thought to be regulated through mechanical feedback, where bending and the resulting stresses in the axoneme feedback to coordinate motor activity[21,22]. Several theoretical models have described how this mechanical feedback operates in these systems, thereby allowing the flagellar beat to respond to changes in external mechanical load[21-24]. Experiments in motile flagellar systems have demonstrated load-dependent changes in flagellar oscillations, while studies of mammalian sperm have shown that increasing viscous loading can alter flagellar waveform organization and bend propagation[25-27]. Such responses can involve changes in waveform amplitude and curvature, beat frequency, wavelength, and wave propagation, all of which influence how the mechanical wave develops and travels along the flagellum[26-28]. Previous studies of mechanical loading, however, have predominantly varied loading through the surrounding fluid, whereas the consequences of mechanical loading from a deformable solid boundary remain poorly understood. These findings, together with the possibility of mechanical interactions through indentation, suggest that boundary compliance could alter flagellar beating dynamics.

The tissues lining the female reproductive tract are mechanically compliant and exhibit elastic moduli in the kilopascals range ($E \sim 0.5 - 10\ kPa$) that vary with anatomical location and physiological state[29,30]. Yet, typical lab studies of sperm movement utilize much stiffer substrates such as glass, which has a Young's modulus of approximately 74 GPa [31]. Recently, soft hydrogel surfaces have been studied for sperm adhesion and selection, and interactions with these materials have been shown to affect sperm attachment and flagellar motion[32-34]. However, these studies have primarily focused on sperm selection and adhesive behavior rather than quantitatively examining how boundary compliance influences flagellar beating[34]. Therefore, how mechanically compliant interfaces influence sperm flagellar dynamics and overall cell motility remains to be fully elucidated.

Here, we investigate how solid substrates with physiologically relevant stiffness influence bovine sperm motility and flagellar dynamics in a viscoelastic polymeric solution (0.5% methylcellulose). We compared sperm movement near a compliant polyethylene glycol diacrylate (PEGDA) hydrogel (Young's modulus ≈ 1.1 kPa) interface with movement near comparatively rigid glass and polydimethylsiloxane (PDMS) surfaces. Using high-speed imaging together with quantitative trajectory and flagellar-waveform analysis, we characterized both sperm movement and the spatial, temporal, and propagative organization of the flagellar beat. We found pronounced substrate-dependent differences in flagellar dynamics, with sperm adjacent to the compliant PEGDA interface showing increased waveform amplitudes and reduced beat frequencies relative to rigid-surface conditions. On examining the bend propagation along the flagellum, we further found that wave-propagation speed does not differ significantly among substrates despite substantial differences in other characteristics of the flagellar beat. Together, these findings demonstrate that the mechanical properties of nearby interfaces influence flagellar beating and highlight the need to incorporate mechanically relevant boundaries in sperm motility studies. This distinction may also have implications for conventional semen analysis, where sperm motility is a key factor in predicting male fertility. Typically, motility is assessed microscopically in samples placed between rigid glass surfaces in a simplified fluid medium, and conventional semen parameters do not fully predict male

infertility, as apparently normal semen analysis may be observed in cases of unexplained infertility[35]. Assessing motility only at rigid interfaces in simple aqueous media may overlook aspects of sperm behavior that are sensitive to mechanical conditions and emerge near more compliant boundaries.

Results

Mechanical Characterization of the Compliant PEGDA Substrate

To investigate how a mechanically compliant surface affects sperm motility, we fabricated a 120 μm-thick PEGDA hydrogel layer on a glass slide (Fig. 1a; see Methods). The hydrogel layer provided a mechanically compliant, optically transparent substrate for high-speed imaging of sperm motility near the surface under a layer of approximately 80 μm of 0.5% methylcellulose dissolved in standard bovine sperm medium (Fig. 1b). To characterize the mechanical properties of the hydrogel, we performed oscillatory rheology measurements. An initial amplitude sweep identified the linear viscoelastic region (LVR), whose upper limit was approximately 13.4% strain (Supplementary Fig.S1). We then conducted a frequency sweep at 0.1% shear strain. Throughout the measured frequency range, the storage modulus (G') remained substantially greater than the loss modulus (G''), indicating predominantly elastic behavior with minimal frequency dependence (Fig. 1c). At 6.28 rad/s (1 Hz), the hydrogel exhibited a storage modulus of 380 ± 70 Pa (mean ± SD, n = 3), corresponding to an estimated Young's modulus of 1.1 ± 0.2 kPa assuming incompressibility ($E \approx 3G'$)[36]. The measured stiffness falls within the reported range of reproductive tract tissues (~0.5–10 kPa)[29,30].

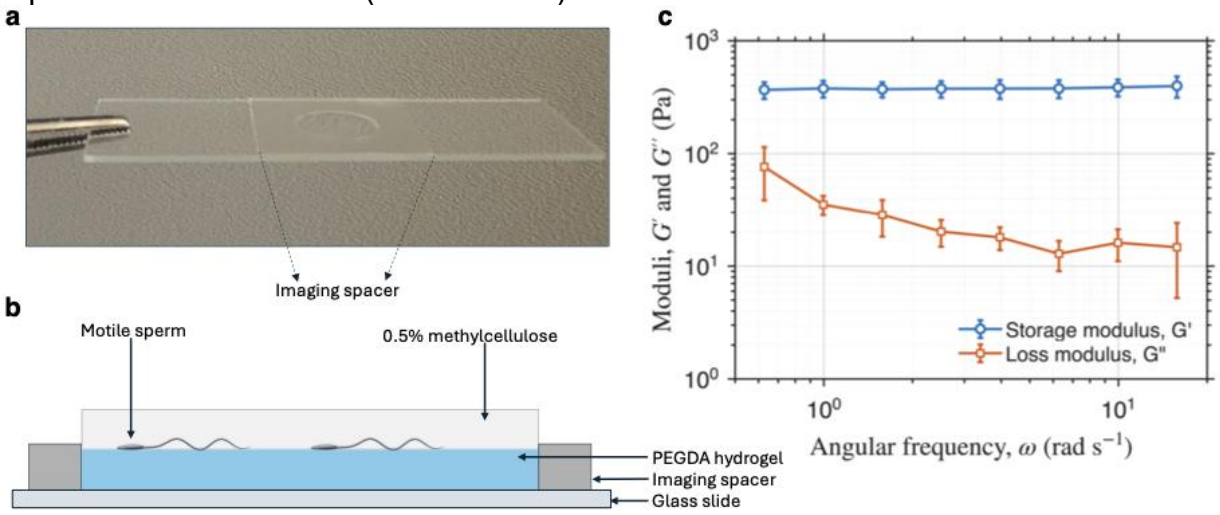


Fig. 1 PEGDA hydrogel substrate and experimental configuration. (a) Spacer-defined PEGDA hydrogel substrate fabricated on a glass slide, with a hydrogel thickness of 120 μm. (b) Cross-sectional schematic of the experimental chamber showing motile bovine sperm adjacent to the PEGDA hydrogel surface in 0.5% methylcellulose solution. We formed the PEGDA hydrogel within the imaging spacer on a glass slide. (c) Oscillatory frequency sweep of the PEGDA hydrogel performed at 0.1% shear strain, within the linear viscoelastic region (LVR). Amplitude-sweep measurements identified an upper LVR strain limit of approximately 13.4% based on a 5% deviation criterion for G. We conducted measurements at 38.5 °C using three independent hydrogel samples. The storage modulus (G') remained substantially greater than the loss modulus (G″) throughout the measured frequency range (0.628–15.8 rad s^{-1}), indicating a predominantly elastic behavior. At 1 Hz, storage modulus G "was approximately 380±70 Pa, corresponding to an estimated Young's modulus of approximately 1.1±0.2 kPa (assuming $E \approx 3G'$). Data are presented as mean ± SD (n = 3 independent hydrogel samples).

Compared with glass substrates ($E \approx 74$ GPa)[31] and PDMS ($E \approx 1-3\,MPa$)[37], the PEGDA hydrogel ($E \approx 1.1$kPa provided a substantially softer, tissue-relevant environment for sperm locomotion[29,30]. The characterized hydrogel substrate therefore enabled us to investigate sperm motility and flagellar waveform dynamics under conditions that closely reflect the mechanical compliance of reproductive tissues.

Soft PEGDA substrates enhance visualization of sperm flagellar waveform

Our first observation with the compliant substrate was that it improved the visualization of sperm near the surface. Under identical microscope and camera settings, sperm imaged adjacent to glass was less clearly resolved (Fig. 2a), whereas sperm imaged adjacent to soft PEGDA exhibited a smoother optical background and a more clearly resolved flagellar contour (Fig. 2b). The difference was particularly apparent toward the distal flagellum, where the progressively tapering structure was easier to distinguish from the surrounding background on PEGDA.

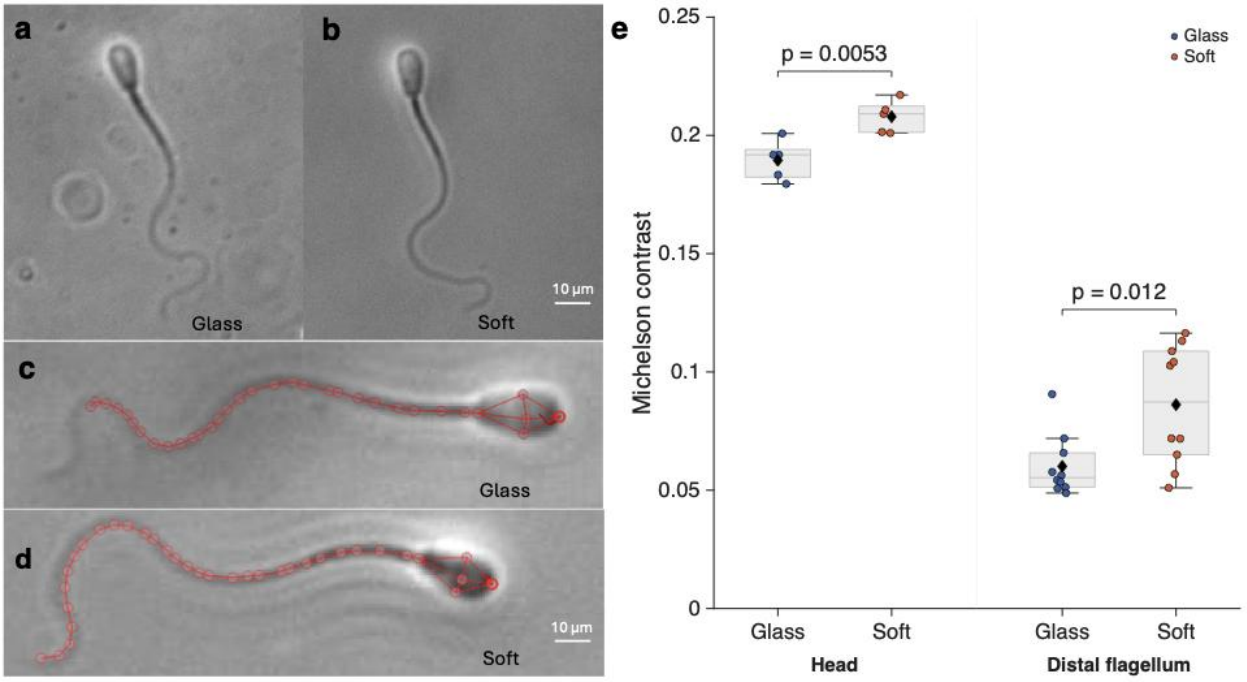


Fig. 2. Improved visualization and tracking of the sperm flagellum on compliant PEGDA substrates. Representative phase-contrast images of bovine sperm moving adjacent to glass (a) and soft PEGDA (b), acquired under identical microscope and camera settings. Quantitative intensity-profile analysis of the original unprocessed images showed improved distal flagellar image quality on soft PEGDA, including higher Michelson and Weber contrast, greater peak-to-trough intensity modulation, and higher contrast-to-noise ratio (CNR). (c,d) Representative SLEAP-based centerline reconstructions obtained using the same pretrained model and inference workflow on glass and soft PEGDA. Improved distal flagellar visibility on soft PEGDA facilitated continuous recovery of the flagellar centerline for subsequent waveform analysis. Scale bars, 10 µm. (e) Quantification of Michelson contrast for the sperm head and distal flagellum. Head contrast was modestly higher on soft PEGDA than on glass (0.208 ± 0.007 vs. 0.189 ± 0.008). Distal flagellar contrast increased from 0.060 ± 0.013 on glass to 0.086 ± 0.025 on soft PEGDA (n = 10 independent measurements per condition; p = 0.012), corresponding to an approximately 43% increase. Values are represented as mean ± SD.

The improved distal flagellar visibility was also evident in SLEAP-based reconstruction of the flagellar centerline (Fig. 2b)[18]. We used the same pretrained model and inference workflow for both substrates, and SLEAP was automatically able to track the head and proximal flagellum under both conditions. However, the improved visibility of the distal flagellum on PEGDA allowed for more continuous recovery of distal landmarks. In contrast, those tracked on the glass surface required manual correction, especially in the distal region before subsequent waveform analysis (Fig. 2c, d). Thus, the compliant PEGDA substrate provided a clear optical advantage for resolving the distal flagellum, which enabled us to reconstruct the complete flagellar waveform used for subsequent quantitative analysis of sperm beating dynamics. Quantitative intensity-profile analysis of the original unprocessed images confirmed this observation, with increased Michelson contrast and higher contrast-to-noise ratio (CNR) on PEGDA substrate. As illustrated in Fig. 2e, Michelson contrast was quantified across independent measurements of the sperm head and distal flagellum. Head contrast increased modestly from 0.189 ± 0.008 on glass to 0.208 ± 0.007 on soft PEGDA (n = 10 per condition, p = 0.0053). The enhancement was more pronounced for the distal flagellum, where Michelson contrast increased from 0.060 ± 0.013 on glass to 0.086 ± 0.025 on soft PEGDA (n = 10 per condition, p = 0.012), an approximate 43% increase.

Substrate compliance increases flagellar bending amplitude and alters its spatial development along the flagellum

We examined whether substrate compliance influenced the flagellar waveform by quantifying waveforms using centerlines obtained from SLEAP. For this analysis, we tracked thirty sequential landmarks along the flagellum, which allowed us to study the motion in a spatially resolved manner (Fig. 3). We fitted a smooth B-spline centerline to the valid tracked landmarks (cyan curve, Fig. 3a) and defined position along the reconstructed flagellum by arc length, s ≈11 μm, 27 μm, and 51 μm measured from the proximal end[18]. At each position, we measured the lateral displacement perpendicular to the head–neck reference axis (yellow arrows, Fig. 3a) and calculated the amplitude as half the difference between the 95th and 5th percentiles, $A(s) = \frac{P_{95}(y(s,t)) - P_5(y(s,t))}{2}$, where $y(s,t)$ is the five-frame running-median–smoothed lateral displacement, and P_{95} and P_5 are percentiles taken over all frames t.

See Supplementary Fig.S2 for representative $y(t)$ traces and further detail on the amplitude measurement.

Our observations indicate that the lateral excursions of the flagellum were greater on soft PEGDA substrates compared to glass or PDMS (Fig. 3b–d; Supplementary Movies 1–3). Our quantitative analysis indicates that the flagellar amplitude varies significantly across different substrates in the proximal, mid, and distal regions, as confirmed by one-way ANOVA (p-values: 6.34×10^{-9}, 1.72×10^{-5} and 3.36×10^{-7}, respectively; see Fig. 3e–g). Further, the Tukey–Kramer post hoc test shows that amplitudes are consistently higher on soft PEGDA than on both glass and PDMS in all three regions. However, there is no significant difference between glass and PDMS at the proximal ($p = 0.051$), mid ($p = 0.090$), or distal ($p = 0.402$) regions.

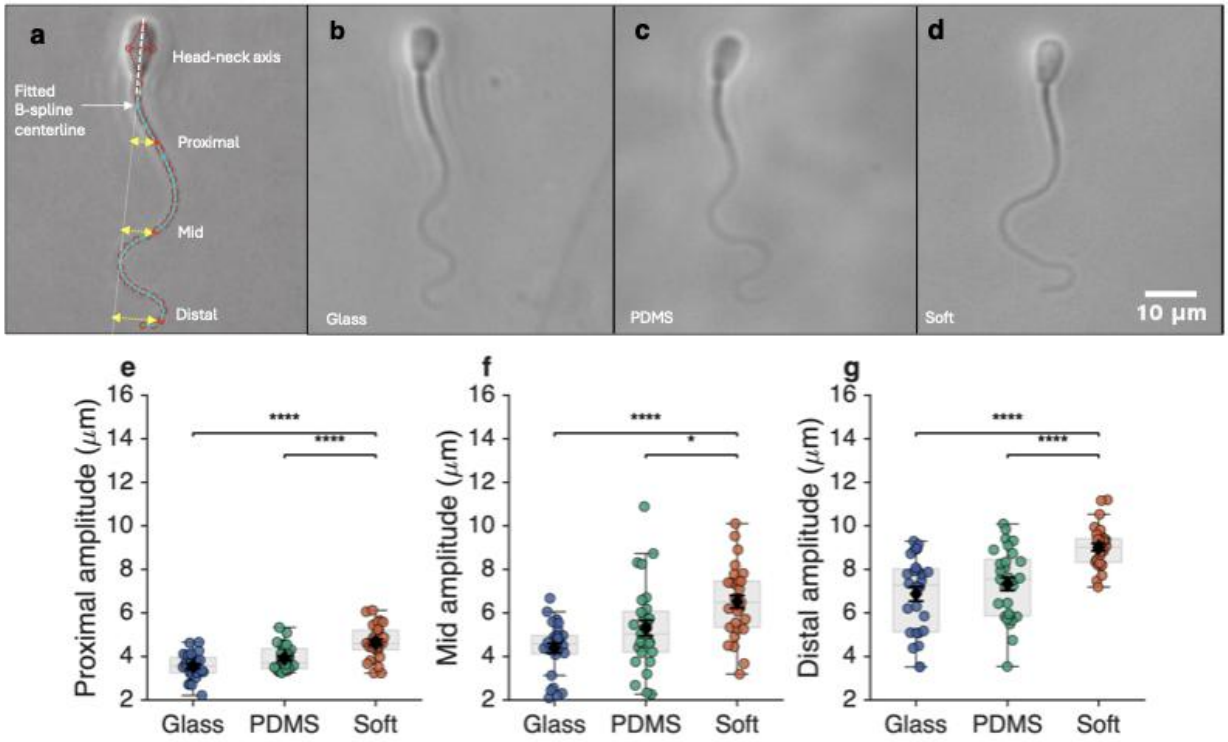


Fig. 3. Flagellar beat amplitudes measured on rigid and compliant substrates. (a) Representative SLEAP-tracked sperm showing the instantaneous head–neck reference axis and the fitted B-spline centerline used for amplitude analysis. We defined position along the centerline by arc length, s, measured from the proximal end (neck). Proximal, mid, and distal amplitudes were evaluated on the fitted spline at arc-length positions s ≈ 11, 27, and 51 µm, respectively. At each frame, the signed lateral displacement $y(s,t)$was measured perpendicular to the instantaneous head–neck axis. Flagellar amplitude at each position was calculated from the smoothed $A(s) = \frac{P_{95}(y(s,t)) - P_5(y(s,t))}{2}$, where P_{95} and P_5 are the 95th and 5th percentiles across frames. Yellow arrows schematically indicate the lateral-displacement direction and are not drawn to scale. Representative $y(t)$ traces illustrating amplitude measurement are shown in Supplementary Fig. S2. (b–d) Representative sperm waveforms on (b) glass, (c) PDMS, and (d) soft PEGDA substrates. Scale bar, 10 µm. (e–g) Quantification of (e) proximal, (f) mid, and (g) distal flagellar amplitudes for sperm moving on glass (n = 28), PDMS (n = 29), and soft PEGDA (n = 30) substrates. Amplitudes were significantly greater on soft PEGDA than on glass or PDMS at all three flagellar regions, whereas no significant differences were observed between glass and PDMS. Statistical comparisons were performed separately for each region using one-way ANOVA followed by Tukey–Kramer multiple-comparison tests.

Flagellar amplitude increased from the proximal toward the distal region under all three substrate conditions. To determine whether this spatial development of the waveform was different in the substrates, we normalized the mid and distal amplitudes of each sperm to its own proximal amplitude. The normalized distal amplitudes were 1.9 ± 0.4, 1.9 ± 0.3, and 2.0 ± 0.3 for glass, PDMS, and soft PEGDA, respectively (mean ± SD), with no significant difference among substrates (one-way ANOVA, $p = 0.81$, $p = 0.447$). Similarly, the normalized mid-flagellar amplitudes were 1.2 ± 0.3, 1.3 ± 0.4, and 1.4 ± 0.3, respectively, and did not differ significantly among substrates ($p = 1.97$, $p = 0.146$). Thus, although absolute flagellar amplitudes were greater on soft PEGDA, the relative spatial increase in amplitude along the flagellum was broadly similar across substrate conditions.

Soft substrates reduce flagellar beat frequency while preserving wave propagation

To determine whether the substrate-dependent changes in flagellar amplitude were accompanied by changes in the temporal and spatial characteristics of the beat, flagellar wave dynamics were quantified from SLEAP-derived centerlines. Signed curvature, $\kappa(s,t)$, was calculated along the flagellum as $d\theta/ds$ while $\theta(s,t)$ is the local tangent angle and s is arc length. Representative curvature kymographs for sperm moving adjacent to glass, PDMS, and soft PEGDA substrates showed alternating bands of positive and negative curvature that progressed along the flagellum with time (Supplementary Fig.S3), with a representative signed-curvature kymograph from a sperm cell moving adjacent to soft PEGDA, shown in Fig. 4a. The angle of these bands corresponded to the speed of the wave propagation from the proximal toward the distal flagellum. To quantitatively resolve the temporal and spatial components of the propagating wave, two-dimensional Fourier analysis was applied to $\kappa(s,t)$. The resulting frequency–wavenumber spectra showed localized dominant spectral peaks representing the principal traveling-wave component (Fig. 4b). The temporal coordinate of each peak defined the dominant frequency, f, while the spatial coordinate defined the dominant spatial frequency. These quantities were expressed as angular frequency, $\omega = 2\pi f$, and wavenumber k, respectively. The corresponding wavelength was calculated as $\lambda = 2\pi/|k|$ while peak values in both ω and k yield the wave speed, $v_s = \omega/|k|$, which is consistent with the slope on the kymograph. The sign of k provides the direction of propagation under the coordinate convention used in the analysis. Here, the negative k corresponded to base-to-tip wave propagation, consistent with the propagating curvature bands observed in the kymographs.

We first examined the temporal consistency of the beat along the flagellum using one-dimensional curvature power spectra at three centerline positions across all substrate conditions. We evaluated the spectra at approximately 12, 24, and 36 μm, which generally exhibited a common dominant peak within each cell (4c- e). For example, the representative soft-substrate cell displayed closely aligned spectral peaks at approximately 15–16 Hz at all three positions (Fig. 4e), indicating that the dominant temporal frequency components were maintained along the analyzed flagellar length and that waves at different k traveled at the same speed, suggesting nondispersive propagation.

To compare the spectral profiles relative to the peak beat frequency, representative spectra from glass, PDMS, and soft PEGDA were normalized by their respective dominant peak frequencies and peak powers (Fig. 4f). Following normalization, the dominant peaks were centered at $\frac{f}{f_{peak}} = 1$ and showed broadly similar localized spectral profiles across the three substrate conditions, indicating thatthe peak frequency captures the dominant variation between spectra. At the population level, dominant beat frequency differed significantly among substrate conditions (Fig. 4g). PDMS exhibited the highest dominant frequencies, soft PEGDA the lowest, and glass intermediate values. In contrast, wave propagation speed v_s did not differ significantly among glass, PDMS, and soft PEGDA (Fig. 4h). Thus, substrate-dependent changes in dominant beat frequency were not accompanied by corresponding significant differences in the speed at which the wave propagated along the flagellum.

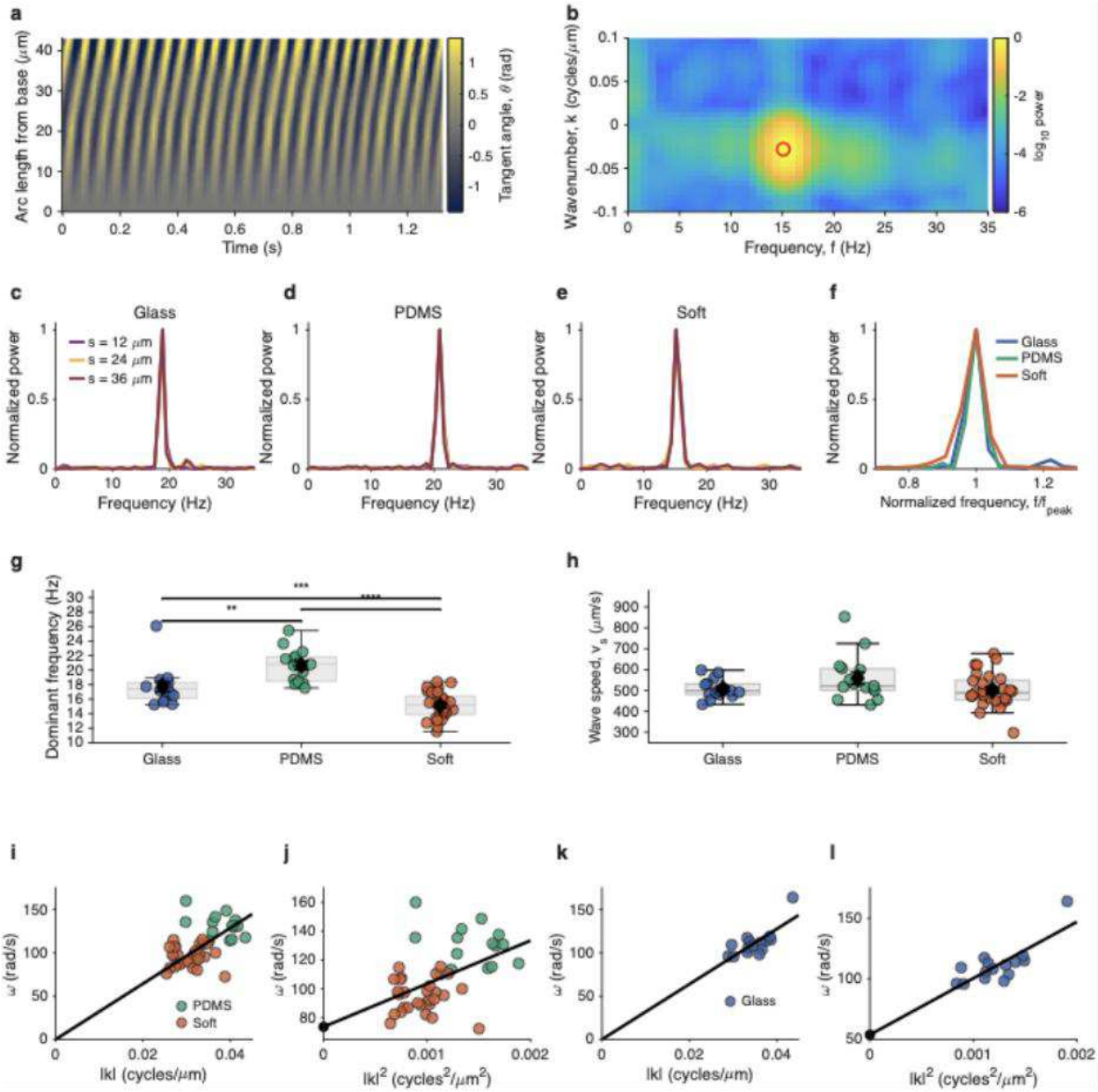


Fig. 4. Flagellar wave propagation across substrates. (a) Representative signed-curvature kymograph, $\kappa(s,t)$ for a sperm cell on a soft substrate, showing bending waves from base to tip. (b) Corresponding two-dimensional power spectrum in the frequency–wavenumber plane; the red circle indicates the dominant spectral peak used to determine the beat frequency f and wavenumber k. Under the coordinate convention used, the negative k value corresponds to base-to-tip wave propagation. (c–e) Normalized curvature power spectra at three arc-length positions (s=12, 24 and 36 μm) for representative cells on glass (c), PDMS (d), and soft PEGDA (e); the dominant frequency was consistent along the flagellum within each representative cell. (f) Representative spectra overlaid across substrates after normalization of frequency by the respective dominant peak frequency f/f_{peak} and power by the respective peak power; showing comparable peak profiles centered at $\frac{f}{f_{peak}} = 1$ for all three substrate conditions. (g) Comparison of dominant beat frequencies by substrate. Beat frequency differed significantly among substrates. (h)Wave propagation speed v_s by substrate; propagation speed did not differ significantly among conditions, despite differences in dominant beat frequency. (i–l) Frequency–wavenumber relationships expressed in terms of angular frequency, $\omega = 2\pi f$. For pooled PDMS and soft PEGDA data (n = 45), ω is shown as a function of $|k|$ with

the fit constrained through the origin (i) (centered $R^2 = .135$) and as a function of $|k|^2$ with a free-intercept linear fit (j) centered $R^2 = 0.223$). The latter yielded a finite zero-wavenumber intercept of 73.2 rad s^{-1} (95% CI, 53.5–92.9 rad s^{-1}) or 11.6 Hz (95% CI, 8.5–14.8 Hz), roughly the lower end of the measured beat frequency range. glass was analyzed separately in the corresponding relationships: ω as a function of $|k|$ with a fit constrained through the origin (k) (centered $R^2 = 0.571$) and ω as a function of $|k|^2$with a free-intercept linear fit (l) ($\text{centered } R^2 = 0.621$); the fitted zero-wavenumber intercept was ω_0=53.9 rad s^{-1}(95% CI, 26.3–81.4 rad s-^{1}) or 8.6 Hz (95% CI, 4.2–13.0 Hz).

Because we believe the sperm flagellum caused indentation on both PDMS and our soft substrate surface but not on the glass surface, we treat glass data separately from the PDMS and soft data. Our goal here is to see whether we can draw any conclusion on a possible dispersion relation $\omega(k)$, where angular frequency, $\omega = 2\pi f$, and wavenumber magnitude, $|k|$. A massless wave propagation has a dispersion relation of $\omega = v_s k$, while a nonrelativistic particle has $\omega = \omega_0 + bk^2$[38]. Therefore, we prepare two presentations for comparison, one with an origin-constrained linear fit of ω as a function of $| k |^2$, and the other as a function of $| k |^2$ using a free-intercept linear fit. For the aggregate of PDMS and soft data, the origin-constrained $\omega - |k|$ yielded a slope of 3193 (95% CI, 3016–3369) and a centered $R^2 = 0.135$ (Fig. 4i). When the same data were evaluated as a function of $|k|^2$, the fitted slope was 2.96×10^4 (95% CI, 1.26×10^4–4.66×10^4), with a centered $R^2 = 0.223$ (Fig. 4j). This fit yielded an estimated zero-wavenumber intercept of $\omega_0 = 73.2$ rad s^{-1} (95% CI, 53.5–92.9 rad s^{-1}), corresponding to 11.6 Hz (95% CI, 8.5-14.8 Hz), approximately at the lower end of the measured frequency range.

We examined the corresponding relationships separately for glass (n=15). For the origin-constrained $\omega - |k|$ relationship, the fitted slope was 3188 (95% CI, 3019–3356), with a centered $R^2 = 0.571$ (Fig. 4k). The free-intercept $\omega - |k|^2$ fit yielded a slope of 4.66×10^4 (95% CI, 2.48 ×10^4–6.83×10^4) and a centered $R^2 = 0.621$ (Fig. 4l). The fitted zero-wavenumber intercept for glass was $\omega_0 = 53.9$ rad s^{-1} (95% CI, 26.3–81.4 rad s^{-1}), corresponding to 8.6 Hz (95% CI, 4.2–13.0 Hz). Due to the highly scattered nature of our data, it is not possible for us to conclude the relationship between ω and $|k|$, although it does not appear that our data are more scattered than the literature[38]. To measure a true dispersion relation, we ought to be able to artificially control the frequency of the wave and observe its propagation. Here, we relied on the intrinsic beat frequencies of sperm f, and since different sperm had different v_s, the data became scattered and difficult for us to make further mechanistic conclusions.

Kinematics differ across substrate conditions but are not correlated with wave speed or frequency

We assessed sperm velocity metrics across different substrate conditions to compare whether substrate compliance influences sperm motility. Specifically, we examined curvilinear velocity (VCL), straight-line velocity (VSL), and linearity (LIN) for sperm moving adjacent to glass (n=32), PDMS (n=31), and soft PEGDA substrates (n = 33) (Fig. 5a-d). Our one-way ANOVA indicated significant differences among the substrate conditions for both VCL ($p = 5.03 \times 10^{-13}$) and VSL ($p = 6.40 \times 10^{-12}$)), whereas LIN did not differ significantly among substrates ($p = 0.0972$).

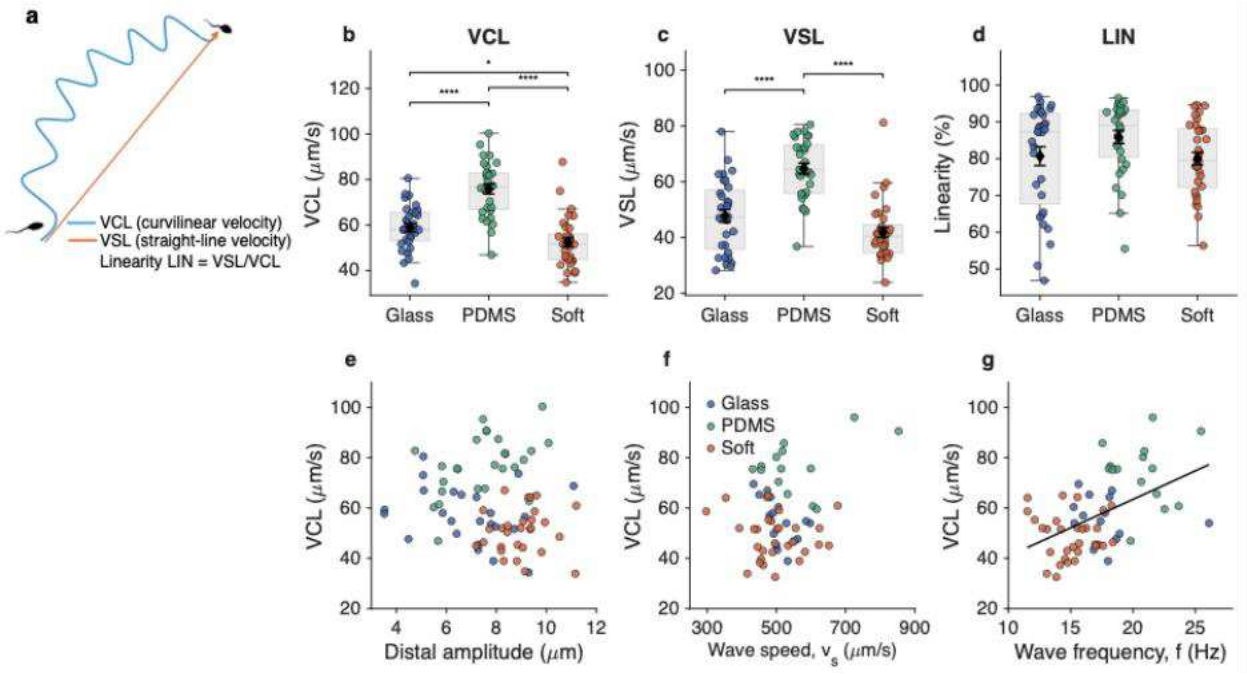


Fig. 5 Sperm velocity metrics across substrate conditions and their relationship with flagellar wave dynamics. a. Schematic illustrating curvilinear velocity (VCL), straight-line velocity (VSL), and linearity (LIN). VCL was calculated from the distance traveled along the curvilinear path (blue), whereas VSL was calculated from the straight-line displacement between the initial and final positions (orange); linearity was calculated as LIN = VSL/VCL × 100%. Trajectory-based velocity metrics were calculated over approximately 2.0 s recordings. b–d. Box plots showing curvilinear velocity (VCL, b), straight-line velocity (VSL, c), and linearity (LIN, d) for sperm moving adjacent to glass (n=32), PDMS (n=31), and soft PEGDA substrates (n= 33). One-way ANOVA revealed significant differences among substrate conditions for VCL ($p = 5.03 \times 10^{-13}$) and VSL ($p = 6.40 \times 10^{-12}$), whereas LIN did not show significant differences ($p = 0.0972$). Post hoc comparisons revealed significant pairwise differences in VCL between all substrate pairs. For VSL,PDMS differed significantly from both glass and soft PEGDA, whereas glass and soft PEGDA did not differ significantly. The effect on linearity was not significant between any pairs. e) Relationships between VCL and distal flagellar amplitudes for sperm adjacent to glass (blue), PDMS (green) and soft PEGDA (orange). Each point represents the VCL and amplitude for an individual sperm. For distal region, we detected a statistically significant positive correlation between VCL and distal amplitude on PDMS ($p < 0.05$). No statistically significant relationship was observed on glass ($p > 0.05$), and there was no statistically significant association on soft PEGDA ($p > 0.05$). f,g.Relationships between cell velocity and flagellar dynamics. VCL as a function of the flagellar wave-propagation speed ($v_s; f$) and dominant flagellar wave frequency (f; g). Wave parameters were obtained from two-dimensional Fourier analysis of curvature kymographs $v_s = f\lambda$. Each point represents an individual sperm for which trajectory-based VCL, and the corresponding flagellar wave parameters were obtained from the same recording. Pearson correlation analysis showed negative correlation between VCL with v_s on glass ($r = -0.529, p = 0.0426$), whereas no significant VCL-v_s relationship was observed on PDMS or soft PEGDA ($p > 0.05$ for both comparisons). No significant relationship between VCL and dominant frequency was detected within any individual substrate condition. However, when all substrate conditions were pooled, VCL exhibited a significant positive association with dominant wave frequency ($r = 0.499, R^2 = 0.249, p < 0.0001, n = 60$); the solid line in (g) indicates the pooled linear regression.

With respect to VCL, we observed that sperm moving on PDMS showed significantly higher velocities than those on glass ($p < 0.001$) or on soft PEGDA substrates ($p < 0.0001$). There was also a modest but significant difference between glass and soft substrates ($p < 0.0477$), with glass supporting slightly higher VCL values.

The median VCL values were 76.67 μm/s for PDMS, 57.97 μm/s for glass, and 51.68 μm/s for soft PEGDA.

VSL showed a similar trend. Sperm moving on PDMS demonstrated significantly higher straight-line velocities than on glass ($p < 0.0001$) or soft PEGDA substrates ($p < 0.0001$). Glass showed modestly higher median VSL values than soft PEGDA ($p = 0.101$). The median VSL values were 64.36 μm/s for PDMS, 47.31 μm/s for glass, and 40.34 μm/s for soft PEGDA.

In contrast, linearity appeared relatively unaffected by the substrate condition. We did not observe significant differences between glass and PDMS ($p = 0.189$) or between glass and soft PEGDA ($p = 0.114$), or between PDMS and soft PEGDA ($p = 0.114$). Thus, although compliance modifies the waveform, it does not appear to shift the trajectory type.

We examined the relationship between VCL and amplitude across all flagellar regions; results for the proximal and mid regions are provided in Supplementary Fig. S4. Here, focusing on the distal region, we found a positive correlation between VCL and amplitude on PDMS ($r = 0.477, p = 0.0137$). In contrast, no statistically significant relationship was found on glass ($r = -0.201, p = 0.346$), and there was no statistically significant association on soft PEGDA ($r = 0.056$, $p = 0.772$).

To determine whether variations in flagellar wave dynamics were associated with the cell velocity, VCL was compared with wave-propagation speed, v_s and dominant wave frequency, f, on a cell-by-cell basis (Fig. 5 f,g). A significant negative correlation was observed between VCL and wave-propagation speed on glass ($r = -0.529$, $p = 0.0426$). In contrast, no significant correlation was observed on PDMS ($r = 0.305$, $p = 0.270$) or PEGDA ($r = -0.108$, $p = 0.570$). Similarly, VCL was not significantly correlated with dominant frequency f on glass ($r = -0.173$, $p = 0.537$), PDMS ($r = -0.006$, $p = 0.982$), or the soft PEGDA ($r = -0.028, p = 0.882$).

However, when all cells were pooled across substrate conditions, VCL exhibited a positive correlation with dominant wave frequency ($r = 0.499$, $R^2 = 0.249$, $p = 4.99 \times 10^{-5}$, n=60; Fig. 5g). The pooled linear fit was $VCL = 2.363f + 18.180$. Although differences in dominant frequency between cells did not predict VCL within each substrate condition, the combined data showed that higher dominant wave frequency was generally linked to higher cell velocity across all substrate conditions.

Discussion

It is now well known that mammalian sperm movement is influenced by fluid rheology[26,27], confinement[5,16], and nearby boundaries[10,13]. In our recent study, we observed that in a polymeric solution, bovine sperm maintain sustained physical interactions with nearby solid surfaces during locomotion, with portions of the flagellar segments sliding along the substrate, thereby contributing to propulsion through kinetic friction at the flagellar-surface contact[17]. This finding led us to investigate how the mechanical properties of that boundary influence flagellar dynamics. The results of the current study now provide experimental evidence that substrate compliance significantly changes the flagellar waveform and is an important regulator of sperm motility that has largely been overlooked in conventional rigid-surface assays.

In this study, we observed that substrate compliance alters flagellar waveform dynamics in bovine sperm. Specifically, we found that a soft PEGDA hydrogel substrate,

which closely matches the elastic modulus of reproductive tract tissue, increases bending amplitude and decreases beat frequency along the entire flagellum. These results show that substrate mechanical properties play an important role in regulating sperm waveform behavior and point to the need for additional elastic coupling in motility models.

One key observation from our study is that the flagellar bending amplitude increased when sperm moved on compliant substrates. This increase was observed across the proximal, mid, and distal regions of the flagellum. In contrast, we did not observe as significant differences in flagellar amplitude between the two more rigid substrates, glass and PDMS. Although we observed an amplitude increase due to compliance along the entire flagellum, it was stronger in the mid region. Notably, median amplitudes increased progressively from glass to PDMS to soft substrates across all flagellar regions, with the largest proportional increase consistently observed in the mid-flagellar region. On glass, the proximal and mid-flagellar amplitudes were found to be nearly the same, suggesting that there is minimal increase in transverse movement along the first half of the flagellum. In comparison, both PDMS and soft PEGDA showed a gradual increase in amplitude from the proximal to the mid-flagellar region, with the most pronounced increase seen on the soft substrate. We suspect this results from surface indentation that led to higher resistance to the flagellum movement in the direction perpendicular to the flagellum, which cannot solely come from the fluid[39].

A reduction in beat frequency accompanied the increase in flagellar amplitude on the soft substrate. Sperm on soft PEGDA exhibited lower dominant frequencies than those on both glass and PDMS, though PDMS exhibited the highest frequencies. The consistent reduction in frequency on the compliant substrate compared to both glass and PDMS indicates that substrate compliance affects not only the spatial characteristics of the waveform but also the temporal dynamics. Despite these differences in beat frequency, bending-wave propagation speed did not differ significantly among substrates. This finding provides information for constraining future flagellar beating models.

The marked changes observed in sperm flagellar waveform dynamics on soft hydrogel compared with glass did not result in a uniform change in translational velocity. Both VCL and VSL reached their highest values on PDMS. On soft PEGDA, VCL was modestly lower than that on glass, but VSL was numerically lower but not significantly different between these substrates. Although VCL and VSL varied significantly across substrates, the pattern of these velocity differences did not match the substrate-dependent changes observed in amplitude and frequency. Based on the proposed role of flagellar indentation on deformable surfaces [18], we hypothesize that flagellar indentation helps sperm locomotion, while on the soft substrate the head might also indent the surface and create drag, which would be consistent with our observation. Additional studies will be needed to clarify the mechanism.

Further, our observations suggest a limited relationship between translational velocity and waveform parameters. We found that VCL showed a positive correlation with distal amplitude only on PDMS, and there was no significant correlation with dominant frequency within any individual substrate condition. The association we see between VCL and beat frequency in the pooled dataset likely stems mainly from differences across substrate conditions. Within each condition, these two parameters do not appear to show a consistent relationship. These observations point to the general lack of understanding

of microswimmer locomotion, particularly when swimmer-surface interaction becomes important.

Beyond substrate stiffness as an environmental factor, the effects seen with PEGDA may arise from mechanical coupling between the beating flagellum and the deformable surface. Compared to glass and PDMS, PEGDA hydrogels are more compliant and may undergo more local deformation during flagellum contact. Such local deformation could modify the reaction forces and the mechanical load on the flagellum as the waveform develops and moves along its length. Because flagellar beating responds to mechanical load, this coupling provides a possible mechanism that could allow substrate compliance to influence both flagellar amplitude and beat frequency[25]. Overall, our work highlights that the flagellar waveform is sensitive to the mechanical conditions sperm encounter *in vivo.* However, most studies and clinical assessments of sperm motility are conducted on rigid glass surfaces, which differ substantially from physiological conditions. These findings therefore have important implications for how sperm samples are assessed experimentally. Since sperm motility arises from the combined dynamics of the flagellar waveform, a comprehensive characterization of flagellar behavior might provide more information than head-based kinematics alone[40,41]. Most clinical and research tests primarily use computer-assisted sperm analysis (CASA) systems to quantify head trajectories and derive kinematic parameters, which are also performed on a rigid surface. The changes in flagellar beating observed in this study, depending on surface softness, suggest that using more natural surface conditions could reveal aspects of sperm function that hard-surface tests miss. Direct assessments of different regions of flagellar movement, enabled by enhanced visibility on the PEGDA substrate, could complement existing motility metrics and provide a more complete characterization of sperm motility[40,41].

Methods

Media preparation

The standard medium used in this study is Tyrode's Albumin Lactate Pyruvate (TALP)[42], which consists of 99 mM NaCl, 3.1 mM KCl, 0.39 mM NaH_2PO_4, 25 mM $NaHCO_3$, 10 mM HEPES free acid, 2 mM $CaCl_2$, 1.1 mM $MgCl_2$, 25.4 mM sodium lactate, 1 mM sodium pyruvate, 50 mg/L gentamicin, and 6 mg/mL bovine serum albumin (BSA). The pH was adjusted to 7.4 using 1 M NaOH. To impart a moderate level of viscoelasticity to the medium, we prepared a 0.5% w/w methyl cellulose (MC) solution in TALP (with a viscosity of 4,000 cP at 2%) and was used across all substrate conditions (glass, PDMS, and PEGDA). The rheological properties of the 0.5% MC medium were characterized separately (see Rheological characterization; Fig. 6).

Sample Preparation

Frozen bovine semen samples (500 µL plastic straws, provided by Select Sires) were stored in liquid nitrogen until use. Semen samples from four individual bulls were used in this study.Samples were thawed in a 37 °C water bath for 30 seconds, then centrifuged through 40% and 80% Bovipure layers in Bovidilute solution at 300 × g for 10 minutes. After centrifugation, the supernatant was removed, and the sperm pellet was resuspended in 3 mL TALP. The suspension was centrifuged again at 300 × g for 3 minutes. The supernatant was removed, and the pellet was resuspended in 350 µL TALP and incubated at 38.5 °C under 5% CO_2 in humidified air until use.

Substrate Preparation

Glass and PDMS substrates were established using PDMS-glass microfluidic devices fabricated using standard soft lithography procedures as described previously[17]. Briefly, PDMS (Sylgard 184, Dow Corning, Midland, MI, USA) was bonded to glass following oxygen plasma treatment to produce devices containing both PDMS and glass surfaces with a channel depth of 500 μm. For the glass condition, sperm were imaged adjacent to the glass surface of the device, whereas for the PDMS condition, sperm were imaged adjacent to the PDMS surface.

PEGDA Hydrogel Preparation

Poly(ethylene glycol) diacrylate (PEGDA, Mn = 700 Da, Sigma-Aldrich, St. Louis, MO, USA), lithium phenyl-2,4,6-trimethylbenzoylphosphinate (LAP photoinitiator, Sigma-Aldrich, St. Louis, MO, USA), and 3-(trimethoxysilyl)propyl methacrylate (TMSPMA, Sigma-Aldrich, St. Louis, MO, USA) were used to prepare the hydrogel.

To prepare the LAP stock solution, 0.1 g of LAP was dissolved in 10 mL of phosphate-buffered saline (PBS, pH 7.4) at 60°C, stirring at 200 rpm for 2 hours in an amber glass bottle to protect it from light. For the PEGDA precursor solution, PEGDA was dissolved at 5% (w/v) in the LAP stock solution. This mixture was stirred at 60°C for 1 hour to ensure complete dissolution and homogeneity, then stored protected from light until further use.

Before hydrogel fabrication, glass microscope slides (75 mm × 25 mm) were cleaned and plasma-treated to activate the surface (Harrick Plasma, PDC-32G, Ithaca, NY, USA) using high RF power for 120 s, then functionalized with TMSPMA using a procedure adapted from a previously reported method[43]. The TMSPMA solution was prepared in 95% ethanol containing glacial acetic acid. The treated slides were rinsed with ethanol, air-dried, and baked at 115°C for 1 hour.

We assembled a 120 μm-deep chamber on the treated slide using a SecureSeal™ imaging spacer (13 mm diameter, 120 μm thickness, Avantor Sciences, Radnor, PA, USA), then dispensed 12 μL of PEGDA precursor solution into the chamber. The hydrogel was then photocrosslinked using a NextDent LC-3DPrint Box UV (3D Systems, Soesterberg, The Netherlands) post-curing unit for 8 minutes, yielding optically transparent, compliant substrates (See Fig.1a). Hydrogel thickness was estimated microscopically by measuring the focal displacement between the glass substrate and the hydrogel surface at multiple locations. The resulting thickness was approximately 100 ± 19 μm.

Rheological characterization

The rheological properties of PEGDA hydrogels and 0.5% methylcellulose solutions were measured using a rotational rheometer MCR 302 (Anton Paar, Graz, Austria). We measured PEGDA hydrogels with an 8 mm parallel-plate geometry and a 0.3 mm plate gap. Oscillatory amplitude sweeps were performed at a constant frequency of 1 Hz to determine the storage modulus (G') and loss modulus (G'') and to identify the linear viscoelastic region. Frequency sweeps were subsequently performed at a strain amplitude of 0.1%, which remained within the linear viscoelastic region.

For the PEGDA hydrogels, the plateau storage modulus within the linear viscoelastic region was used to estimate Young's modulus using the relation $E = 2G(1 + v)$, assuming an incompressible material with a Poisson ratio of 0.5. Oscillatory amplitude-sweep measurements demonstrated that PEGDA behaved as a predominantly

elastic material ($G' >> G''$), yielding an estimated Young's modulus of approximately 1.1 kPa (Fig. 1c).

The rheological properties of the 0.5% methylcellulose solution were characterized separately using a CP50-1 cone-and-plate geometry. Oscillatory frequency sweeps were performed at a strain amplitude of 0.5%, and steady-shear flow sweeps were conducted over shear rates ranging from 1.5 to 140 s^{-1} to determine the apparent viscosity. The storage modulus exhibited frequency-dependent behavior, and the apparent viscosity decreased progressively with increasing shear rate, demonstrating the characteristic shear-thinning behavior of the methylcellulose solution (Fig. 6a,b)

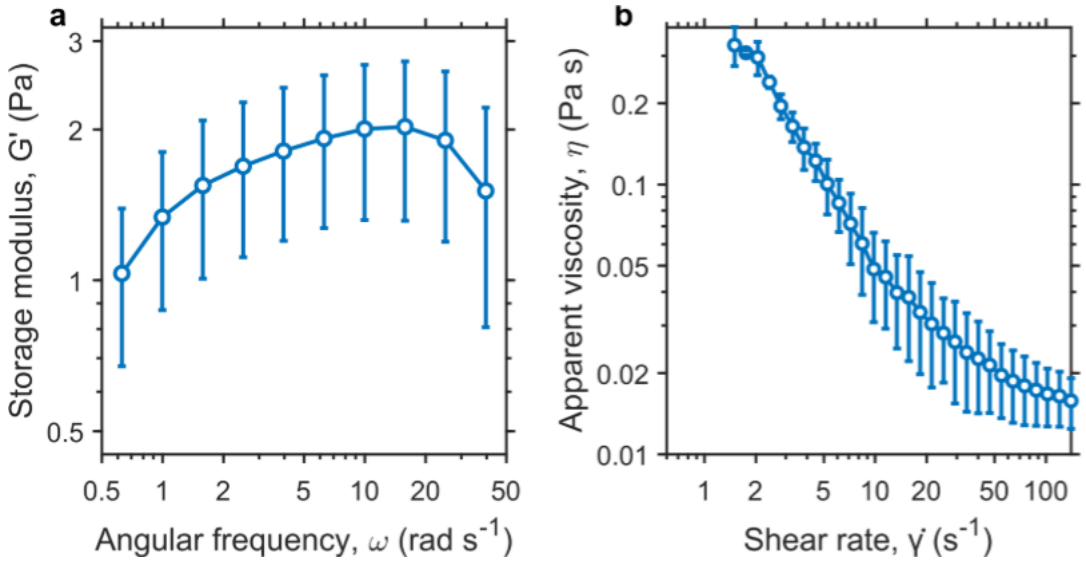


Fig. 6 Rheological characterization of the 0.5% methylcellulose solution. (a) Oscillatory frequency sweep performed at 38.5 °C using a strain amplitude of 0.5%, showing the mean storage modulus (G') as a function of angular frequency. The loss modulus (G") remained lower than (G') over the measured frequency range, approaching (G') at the highest angular frequency. (b) Steady-shear flow sweep showing the apparent viscosity (η) as a function of shear rate. Apparent viscosity decreased from 0.329 ± 0.054 Pa s at 1.5 s^{-1} to 0.0158 ± 0.0034 Pa s at 140 s^{-1}, corresponding to an approximately 20.8-fold decrease. Data are presented as mean ± SD from three independent measurements.

Sperm Motility Imaging

Imaging was performed using a Nikon Eclipse Ti inverted phase-contrast microscope equipped with a 20× objective and a Hamamatsu ORCA-Flash4.0 V3 camera. Microfluidic devices were filled with a 0.5% (w/v) methylcellulose solution (Incubated at 38.5 °C under 5% CO_2 in humidified air for at least 2 hours before the experiments), and a diluted sperm suspension was introduced through the device inlet. The devices were maintained in a temperature-controlled chamber during imaging.

Sufficient time was allowed for motile sperm to migrate away from the inlet region before image acquisition. Videos were recorded using NIS-Elements BR software at 200 frames s^{-1}. To evaluate sperm behavior on glass and PDMS substrates in the device, we adjusted the focal plane to image sperm moving adjacent to either the upper PDMS surface or the lower glass surface.

To observe sperm motility on PEGDA hydrogels, we added 0.5% (w/v) methylcellulose medium to the equilibrated hydrogel surface, then added the diluted

sperm suspension. The hydrogel-coated glass slide was placed in an environmentally controlled chamber (OKO-Touch) set at 38.5°C, with humidity maintained during imaging. Sperm motility on the hydrogel substrate was visualized using a Nikon Eclipse Ti inverted phase-contrast microscope with a 20× objective and a Hamamatsu ORCA-Flash4.0 V3 camera. Videos of sperm movement along the hydrogel surface were recorded at 200 frames per second using NIS-Elements BR software, enabling detailed analysis.

Automated tracking and waveform analysis

We used the Social LEAP Estimates Animal Pose (SLEAP) machine-learning framework to automatically track sperm using pose estimation, as described in our recent work[18]. We established the tracking workflow, model training, and skeleton design to suit our requirements. The nd2 videos were first converted to the AVI format and analyzed using a custom sperm skeleton that included head, midpiece, and flagellar landmarks along the cell (Fig.6). The trained models then predicted the positions of these landmarks for each sperm in each frame, providing time-resolved coordinate data for further kinematic analysis.

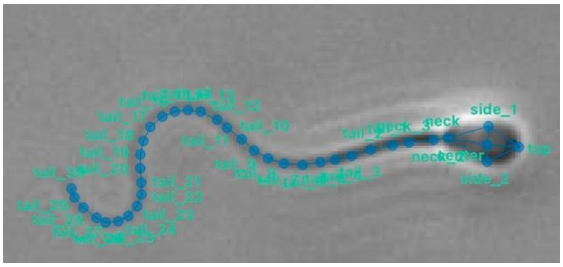


Fig. 6. Automated tracking of the sperm head and flagellum using SLEAP. Representative bovine sperm image showing the SLEAP skeleton and landmark nomenclature used for automated tracking. Flagellar landmarks (tail_1–tail_30) were sequentially distributed from the proximal to distal flagellum. For centerline-based waveform analysis, we tracked flagellar landmarks to reconstruct a continuous centerline for each frame using a B-spline fit. We then parameterized the centerline by arc length, measured from the proximal end of the flagellum, and resampled it onto a uniformly spaced arc-length grid. This approach allowed us to identify corresponding positions along the flagellum across all frames, enabling us to calculate the flagellum's amplitude, curvature, and wave-propagation parameters.

We exported the coordinate data as CSV files and analyzed them using custom MATLAB scripts developed for this purpose. We quantified flagellar kinematics from the tracked centerlines, including regional bending amplitude, dominant beat frequency, and bending-wave propagation characteristics. We evaluated the flagellar amplitude in the proximal, mid, and distal regions of the flagellum from the transverse displacement of tracked flagellar landmarks relative to the local direction of the flagellum. We determined the dominant beat frequency and bending-wave propagation characteristics from the spatiotemporal evolution of flagellar curvature. For the flagellar wave analysis, we calculated signed curvature $\kappa(s,t)$ along the tracked flagellar centerline as a function of arc length and time. One-dimensional curvature power spectra were used to evaluate the dominant temporal frequency at selected positions along the flagellum. Two-dimensional Fourier analysis of $\kappa(s,t)$ was used to determine the dominant frequency f and wavenumber k. Wavelength was calculated as $\lambda = 1/|\,k\,|$, and wave propagation speed

as $v_s = f\lambda$. The sign of k was used to determine the wave-propagation direction, with $k < 0$ corresponding to base-to-tip propagation.

In addition, we calculated standard motility metrics, including curvilinear velocity (VCL), straight-line velocity (VSL), and linearity (LIN).

Data availability

The data that support the findings of this study are included in the paper or the Supplementary Information. Additional videos or data will be made available from the corresponding author upon reasonable request.

References

1. Suarez SS, Pacey A. Sperm transport in the female reproductive tract. *Human Reproduction Update*. 2006;**12**(1):23-37.
2. Fauci LJ, Dillon R. Biofluidmechanics of reproduction. *Annu Rev Fluid Mech*. 2006;**38**:371-394.
3. Suarez SS. Mammalian sperm interactions with the female reproductive tract. *Cell and Tissue Research*. 2016;**363**(1):185-194.
4. Tung C-K, Ardon F, Fiore AG, Suarez SS, Wu M. Cooperative roles of biological flow and surface topography in guiding sperm migration revealed by a microfluidic model. *Lab on a Chip*. 2014;**14**(7):1348-1356.
5. Denissenko P, Kantsler V, Smith DJ, Kirkman-Brown J. Human spermatozoa migration in microchannels reveals boundary-following navigation. *Proceedings of the National Academy of Sciences*. 2012;**109**(21):8007-8010.
6. June Mullins K, Saacke R. Study of the functional anatomy of bovine cervical mucosa with special reference to mucus secretion and sperm transport. *The Anatomical Record*. 1989;**225**(2):106-117.
7. Suarez S, Wu M. Microfluidic devices for the study of sperm migration. *MHR: Basic Science of Reproductive Medicine*. 2017;**23**(4):227-234.
8. Lefebvre R, Chenoweth PJ, Drost M, LeClear CT, MacCubbin M, Dutton JT, Suarez SS. Characterization of the oviductal sperm reservoir in cattle. *Biology of Reproduction*. 1995;**53**(5):1066-1074.
9. Rothschild. Non-random distribution of bull spermatozoa in a drop of sperm suspension. *Nature*. 1963;**198**(488):1221-&.
10. Woolley D. Motility of spermatozoa at surfaces. *Reproduction*. 2003;**126**:259-270.
11. Berke AP, Turner L, Berg HC, Lauga E. Hydrodynamic attraction of swimming microorganisms by surfaces. *Physical Review Letters*. 2008;**101**(3):038102.
12. Smith D, Gaffney E, Blake J, Kirkman-Brown J. Human sperm accumulation near surfaces: a simulation study. *Journal of Fluid Mechanics*. 2009;**621**:289-320.
13. Elgeti J, Kaupp UB, Gompper G. Hydrodynamics of sperm cells near surfaces. *Biophysical Journal*. 2010;**99**(4):1018-1026.
14. Drescher K, Dunkel J, Cisneros LH, Ganguly S, Goldstein RE. Fluid dynamics and noise in bacterial cell–cell and cell–surface scattering. *Proceedings of the National Academy of Sciences*. 2011;**108**(27):10940-10945.

15. Kantsler V, Dunkel J, Polin M, Goldstein RE. Ciliary contact interactions dominate surface scattering of swimming eukaryotes. *Proceedings of the National Academy of Sciences*. 2013;**110**(4):1187-1192.
16. Nosrati R, Driouchi A, Yip CM, Sinton D. Two-dimensional slither swimming of sperm within a micrometre of a surface. *Nature communications*. 2015;**6**(1):1-9.
17. Unnikrishnan S, Scott RL, Ogundele E, Azad MA, Ishimoto K, Suarez SS, Tung CK. Hybrid motility mechanism of sperm at viscoelastic fluid-solid interface. *Scientific Reports*. 2024;**14**(1):21841.
18. Scott RL, Unnikrishnan S, Bolaji A, Achinger L, Avidor-Reiss T, Ishimoto K, Tung C-K. Effective roles of the head and flagellum in sperm motility. *arXiv preprint arXiv:260529050*. 2026.
19. Summers KE, Gibbons I. Adenosine triphosphate-induced sliding of tubules in trypsin-treated flagella of sea-urchin sperm. *Proceedings of the National Academy of Sciences*. 1971;**68**(12):3092-3096.
20. King SM, Sale WS. Fifty years of microtubule sliding in cilia. *Mol Biol Cell*. 2018;**29**(6):698-701.
21. Riedel-Kruse IH, Hilfinger A, Howard J, Jülicher F. How molecular motors shape the flagellar beat. *HFSP Journal*. 2007;**1**(3):192-208.
22. Sartori P, Geyer VF, Scholich A, Jülicher F, Howard J. Dynamic curvature regulation accounts for the symmetric and asymmetric beats of Chlamydomonas flagella. *eLife*. 2016;**5**:e13258.
23. Lindemann CB, Lesich KA. Flagellar and ciliary beating: the proven and the possible. *Journal of Cell Science*. 2010;**123**(4):519-528.
24. Gallagher MT, Kirkman-Brown JC, Smith DJ. Axonemal regulation by curvature explains sperm flagellar waveform modulation. *PNAS Nexus*. 2023;**2**(3):pgad072.
25. Klindt GS, Ruloff C, Wagner C, Friedrich BM. Load response of the flagellar beat. *Physical Review Letters*. 2016;**117**(25):258101.
26. Smith DJ, Gaffney EA, Gadêlha H, Kapur N, Kirkman-Brown JC. Bend propagation in the flagella of migrating human sperm, and its modulation by viscosity. *Cell Motility*. 2009;**66**(4):220-236.
27. Yazdan Parast F, Veeraragavan S, Gaikwad AS, Powar S, Prabhakar R, O'Bryan MK, Nosrati R. Viscous Loading Regulates the Flagellar Energetics of Human and Bull Sperm. *Small Methods*. 2024;**8**(7):e2300928.
28. Gray J, Hancock GJ. The propulsion of sea-urchin spermatozoa. *Journal of Experimental Biology*. 1955;**32**(4):802-814.
29. Franko R, Franko Y, Ribes Martinez E, Ferronato GA, Heinzelmann I, Grechi N, et al. Mechanical properties of native and decellularized reproductive tissues: insights for tissue engineering strategies. *Scientific Reports*. 2024;**14**(1):7347.
30. Bauer M, Mazza E, Jabareen M, Sultan L, Bajka M, Lang U, et al. Assessment of the in vivo biomechanical properties of the human uterine cervix in pregnancy using the aspiration test: a feasibility study. *European Journal of Obstetrics & Gynecology and Reproductive Biology*. 2009;**144**:S77-S81.

31. Chorfa A, Madjoubi MA, Hamidouche M, Bouras N, Rubio J, Rubio F. Glass hardness and elastic modulus determination by nanoindentation using displacement and energy methods. *Ceramics-Silikáty*. 2010;**54**(3):225-234.
32. Liaudat AC, Blois D, Capella V, Morilla G, Rivero R, Barbero C, et al. Bull sperm selection by attachment to hyaluronic acid semi-interpenetrated hydrogels. *Reproduction in Domestic Animals*. 2022;**57**(2):228-232.
33. Blois DA, Liaudat AC, Capella V, Morilla G, Rivero RE, Broglia MF, et al. Interaction between hyaluronic acid semi-interpenetrated hydrogel with bull spermatozoa: studies of sperm attachment–release and sperm quality. *Advanced Materials Interfaces*. 2021;**8**(21):2101155.
34. Ebel FA, Liaudat AC, Blois DA, Capella V, Broglia MF, Barbero CA, et al. Biointerfacial behavior of stallion spermatozoa adhered to hydrogel surfaces: Impact of the hydrogel chemical composition and the culture medium. *Colloids and Surfaces B: Biointerfaces*. 2023;**231**:113575.
35. Pandruvada S, Royfman R, Shah TA, Sindhwani P, Dupree JM, Schon S, Avidor-Reiss T. Lack of trusted diagnostic tools for undetermined male infertility. *J Assist Reprod Genet*. 2021;**38**(2):265-276.
36. Chippada U, Yurke B, Langrana NA. Simultaneous determination of Young's modulus, shear modulus, and Poisson's ratio of soft hydrogels. *Journal of Materials Research*. 2010;**25**(3):545-555.
37. Li S, Zhang J, He J, Liu W, Wang Y, Huang Z, et al. Functional PDMS elastomers: bulk composites, surface engineering, and precision fabrication. *Advanced Science*. 2023;**10**(34):2304506.
38. Pierce CJ, Irvine D, Peng L, Lu X, Lu H, Goldman DI. Dispersion relations for active undulators in overdamped environments. *Physical Review E*. 2026;**113**(6):065413.
39. Friedrich BM, Riedel-Kruse IH, Howard J, Jülicher F. High-precision tracking of sperm swimming fine structure provides strong test of resistive force theory. *Journal of Experimental Biology*. 2010;**213**(8):1226-1234.
40. Cupples G, Gallagher MT, Smith DJ, Kirkman-Brown JC. Heads and tails: requirements for informative and robust computational measures of sperm motility. Paper presented at: XIIIth International Symposium on Spermatology2021.
41. Gallagher MT, Cupples G, Ooi EH, Kirkman-Brown JC, Smith DJ. Rapid sperm capture: high-throughput flagellar waveform analysis. *Human Reproduction*. 2019;**34**(7):1173-1185.
42. Parrish J, Susko-Parrish J, Winer M, First N. Capacitation of bovine sperm by heparin. *Biology of Reproduction*. 1988;**38**(5):1171-1180.
43. Han E, Fei C, Alert R, Copenhagen K, Koch MD, Wingreen NS, Shaevitz JW. Local polar order controls mechanical stress and triggers layer formation in Myxococcus xanthus colonies. *Nature communications*. 2025;**16**(1):952.

Acknowledgements

This work was supported by NSF DMR-2144064 to C.K.T. and NSF CMMI-2100850 and NSF Award 2315654 to SD. Frozen bovine sperm samples were kindly provided by Select

Sires, Inc. Fabrication was performed using the NCSU Nanofabrication Facility (NNF), a member of the North Carolina Research Triangle Nanotechnology Network (RTNN), which is supported by NSF Grant ECCS-1542015 as part of the National Nanotechnology Coordinated Infrastructure (NNCI).

Author Contributions

Conceptualization: S.U., I.H., SD and C.K.T.; Methodology: S.U., I.H., R.L.S., S.C., M.A.A., SD and C.K.T.; Software: R.L.S. and S.U.; Formal analysis: S.U., I.H., SD and C.K.T.; Investigation: S.U., I.H., R.L.S., M.J., S.C., K.M., L.W.; Funding acquisition: C.K.T. and SD; Writing - original draft: S.U.; Writing – review & editing: S.U., I.H., R.L.S., M.J., S.C., K.M., L.W., M.A.A., S.D. and C.K.T.; Visualization: S.U. and I.H.; Supervision: S.D. and C.K.T.

Supplementary Files

This is a list of supplementary files associated with this preprint. Click to download.

- SupplementaryInformation0922.docx
- SupplementaryVideo3.avi
- SupplementaryVideo2.avi
- SupplementaryVideo1.avi